Monthly Notices
of the
ROYAL ASTRONOMICAL SOCIETY

MNRAS **463,** 270–281 (2016)
Advance Access publication 2016 July 18

doi:10.1093/mnras/stw1702

The clustering of dark matter haloes: scale-dependent bias on quasi-linear scales

Charles Jose,[1,2]⋆ Cedric G. Lacey[3] and Carlton M. Baugh[3]

[1]*SB College, Changanassery, Kottayam 686101, Kerala, India*
[2]*IUCAA, Post Bag 4, Pune University Campus, Ganeshkhind, Pune 411007, India*
[3]*Institute for Computational Cosmology, Department of Physics, University of Durham, South Road, Durham DH1 3LE, UK*

Accepted 2016 July 13. Received 2016 July 11; in original form 2015 September 15

ABSTRACT

We investigate the spatial clustering of dark matter haloes, collapsing from 1σ–4σ fluctuations, in the redshift range 0–5 using *N*-body simulations. The halo bias of high redshift haloes ($z \geq 2$) is found to be strongly nonlinear and scale dependent on quasi-linear scales that are larger than their virial radii (0.5–10 Mpc h^{-1}). However, at lower redshifts, the scale dependence of nonlinear bias is weaker and is of the order of a few per cent on quasi-linear scales at $z \sim 0$. We find that the redshift evolution of the scale-dependent bias of dark matter haloes can be expressed as a function of four physical parameters: the peak height of haloes, the nonlinear matter correlation function at the scale of interest, an effective power-law index of the *rms* linear density fluctuations and the matter density of the universe at the given redshift. This suggests that the scale dependence of halo bias is not a universal function of the dark matter power spectrum, which is commonly assumed. We provide a fitting function for the scale-dependent halo bias as a function of these four parameters. Our fit reproduces the simulation results to an accuracy of better than 4 per cent over the redshift range $0 \leq z \leq 5$. We also extend our model by expressing the nonlinear bias as a function of the linear matter correlation function. It is important to incorporate our results into the clustering models of dark matter haloes at any redshift, including those hosting early generations of stars and galaxies before reionization.

Key words: galaxies: haloes – galaxies: statistics – cosmology: theory – large-scale structure of Universe.

1 INTRODUCTION

The spatial distribution of luminous galaxies is a valuable resource for probing cosmology and the physics of galaxy formation. The clustering of the galaxy distribution is shaped by the clustering of the dark matter haloes which host them. The clustering of dark matter haloes can be quantified using the halo bias which describes how dark matter haloes trace the dark matter (Kaiser 1984; Bardeen et al. 1986; Bond et al. 1991). Conventional models assume that the halo bias is related to the underlying dark matter density field in a nonlinear and deterministic fashion (Fry & Gaztanaga 1993). Mo & White (1996) showed that, on large scales, the halo bias can be approximated as a scale-independent function of the mass of the haloes. In particular, they showed that the clustering of dark matter haloes is proportional to that of the dark matter with the constant of proportionality being called the linear halo bias. The approximation for the clustering of haloes using scale-independent, linear bias is expected to be valid on scales larger than the virial radii of haloes where dark matter halo substructure is not important.

However, the simple picture of a scale-independent halo bias has been shown to be inaccurate and various nonlinear and non-local processes result in some degree of scale dependence (Matsubara 1999; Angulo et al. 2005; Cole et al. 2005; Seo & Eisenstein 2005; Huff et al. 2007; Smith, Scoccimarro & Sheth 2007; Angulo, Baugh & Lacey 2008; McDonald & Roy 2009; Desjacques et al. 2010; Musso, Paranjape & Sheth 2013; Paranjape et al. 2013). Incorporating such a scale dependence of halo bias into theoretical models could be crucial for interpreting the clustering of galaxies. While several studies have focused on the scale dependence of the bias on very large scales, its scale dependence on scales larger than the typical virial radii of dark matter haloes is equally interesting. These scales, corresponding to comoving length-scales of 0.1 to a few megaparsecs, are smaller than scales where the matter distribution is still linear and therefore are referred to as quasi-linear scales. The scale dependence of halo bias on these scales arises mainly due to the nonlinear growth of matter fluctuations (Smith et al. 2007) and

⋆ E-mail: charlesmanimala@gmail.com

is difficult to estimate using perturbative approaches because of the nonlinearity of matter density field (Reed et al. 2009).

There have been studies in the literature of deviations from the linear bias approximation on quasi-linear scales using analytic techniques (Scannapieco & Barkana 2002; Iliev et al. 2003; Scannapieco & Thacker 2005) as well as *N*-body simulations (Hamana et al. 2001; Diaferio et al. 2003; Cen et al. 2004; Gao et al. 2005b; Tinker et al. 2005; Angulo et al. 2008; Reed et al. 2009; van den Bosch et al. 2013). In particular, these studies focused on the clustering of dark matter haloes either in the local universe (e.g. Tinker et al. 2005) or at very high redshifts before the reionization of the intergalactic medium (Reed et al. 2009). In general these studies showed that the halo bias is nonlinear and scale dependent on quasi-linear scales, but the scale dependence weakens on large scales. Specifically, Reed et al. (2009) find a strong scale dependence of halo bias on quasi-linear scales for rare dark matter haloes at high redshift, with the scale dependence increasing with the rarity of the halo.

The motivation of this paper is to study the clustering of dark matter haloes with a specific focus on the scale dependence of halo bias on quasi-linear scales. In particular, we will focus on the redshift range 0–5 where, to our knowledge, no such previous studies have been carried out. This will help to gauge the amplitude, scale dependence and evolution of the bias of dark matter haloes for $0 \leq z \leq 5$ and hence bridge the gap between other studies which focus on the epochs before reionization. We will address this issue using *N*-body simulations to measure the dark matter and halo correlation functions in the real space. These measurements will be used to calibrate the nature and evolution of the nonlinear halo bias in the redshift range 0–5 over a range of length-scales. In particular, we find that the bias of dark matter haloes is nonlinear and scale dependent on quasi-linear scales. Furthermore, it is not possible to express this scale dependence in terms of the usual parameterizations and therefore one has to invoke additional parameters.

The organization of this paper is as follows. In Section 2, we compare the halo bias of rare high redshift dark matter haloes computed from analytic models and simulations. In Section 3, using simulations, we probe the scale dependence and redshift evolution of the nonlinear bias of rare haloes in the redshift range 0–5 and obtain a fitting function to describe these effects. We conclude with a brief discussion of our results and their implications in the final section.

2 CLUSTERING OF RARE DARK MATTER HALOES AT HIGH *Z*

In this section, we investigate whether the linear bias model for halo clustering gives a good description of the clustering of high-z dark matter haloes on quasi-linear scales. For this we first describe the linear bias model for halo clustering in Section 2.1. In Section 2.2, we introduce the *N*-body simulations used in our study. The clustering of dark matter haloes estimated from these simulations is then compared with the clustering prediction using the linear bias model.

2.1 The linear bias model for halo clustering

In the linear bias approximation, the cross-correlation between haloes of mass M' and M'' is given by

$$\xi_{\rm hh}(r|M', M'', z) = b(M', z)b(M'', z)\xi_{\rm mm}(r, z), \quad (1)$$

where $\xi_{\rm mm}(r, z)$ is the nonlinear two-point correlation function of matter density contrast at redshift z and $b(M, z)$ is the scale-independent linear bias of haloes of mass M at this redshift. Equation (1) is valid on large scales, where density perturbations grow linearly with redshift (Cooray & Sheth 2002). The two-point matter correlation function is obtained by Fourier transforming the nonlinear matter power spectrum, $P(k, z)$ (Smith et al. 2003)

$$\xi_{\rm mm}(r, z) = \int_0^\infty \frac{{\rm d}k}{2\pi^2}\, k^2\, P(k, z)\, \frac{\sin(kr)}{kr}. \quad (2)$$

It is well known that the scale-independent halo bias can be expressed as a function of the 'peak height', $\nu(M, z) = \delta_c/\sigma(M, z)$, of dark matter haloes (Mo & White 1996; Sheth & Tormen 1999; Sheth, Mo & Tormen 2001; Cooray & Sheth 2002; Tinker et al. 2010). The peak height is a measure of the rarity of haloes (Sheth et al. 2001) with rarer haloes having larger $\nu(M, z)$. Here, $\delta_c = 1.686$ is the critical density for halo collapse and $\sigma(M, z)$ is the *rms* linear density fluctuation on a mass scale M

$$\sigma^2(M, z) = \sigma^2(R, z) = \int_0^\infty \frac{{\rm d}k}{2\pi^2} k^2 P^{\rm lin}(k, z) W^2(k, R), \quad (3)$$

where R is the comoving radius of a sphere containing mass M, $W(k, R)$ is the Fourier transformation of the top hat window function and $P^{\rm lin}(k, z)$ is the linear matter power spectrum.

In particular, for linear halo bias, we use the fitting function of Tinker et al. (2010) which was calibrated against *N*-body simulations and is given by,

$$b(M, z) = b(\nu(M, z)) = 1 - A\frac{\nu^a}{\nu^a + \delta_c^a} + B\nu^b + C\nu^c. \quad (4)$$

Tinker et al. (2010) estimate the free parameters of equation (4) to be $A = 1.0$, $a = 0.132$, $B = 0.183$, $b = 1.5$, $C = 0.265$ and $c = 2.4$. The halo bias given by equation (4) increases with increasing $\nu(M, z)$.

We assume that dark matter haloes which can host galaxies have a spherical overdensity $\Delta = 200$ times the average density of universe.[1] Then, the virial radius r_{200} of a halo of mass M is $M = (4/3)\pi r_{200}^3 \rho_c \Delta$. Under the above assumptions the halo correlation function is

$$1 + \xi_{\rm hh}(r|M', M'', z) = \left[1 + b(M', z)b(M'', z)\xi_{\rm mm}(r)\right] \times \Theta[r - r_{\rm min}(M', M'')], \quad (5)$$

where the function $\Theta[r - r_{\rm min}(M', M'')]$ incorporates halo exclusion to ensure that $\xi^{\rm hh}(r|M', M'', z) = -1$ for $r_{\rm min} = \max[r_{200}(M'), r_{200}(M'')]$.

The two-point correlation function of dark matter haloes in a mass bin $M' \leq M \leq M''$ is given by

$$1 + \xi_{\rm hh}(r|[M', M''], z) = \frac{1}{n^2([M', M''], z)} \int_{M'}^{M''} {\rm d}M_1 \int_{M'}^{M''} {\rm d}M_2 \times n(M')n(M'')\left[1 + \xi_{\rm hh}(r|M_1, M_2, z)\right], \quad (6)$$

where $n([M', M''], z) = \int_{M'}^{M''} {\rm d}M n(M, z)$ is the total number density of haloes in the mass bin $[M', M'']$. For the halo mass function, $n(M, z)$, we use the fitting function of Jenkins et al. (2001) which is in excellent agreement with the mass functions obtained from the simulations used in our study. equation (6) is a reasonable approximation for the usual two-halo term for halo clustering on scales

[1] Tinker et al. (2010) calibrate their fitting function for the large scale bias as a function of Δ. Here, the quoted parameter values are for haloes with $\Delta = 200$.

larger than the virial radii of dark matter haloes (Cooray & Sheth 2002).

The average bias of haloes with mass between M' and M'', on scales bigger than their virial radii can be written as being scale independent and is given by

$$b([M', M''], z) = \frac{1}{n([M', M''], z)} \int_{M'}^{M''} \mathrm{d}M b(M, z) n(M, z). \quad (7)$$

Using this result for the bias in equation (6), we get

$$\xi_{\rm hh}(r|[M', M''], z) = b^2([M', M''], z)\xi_{\rm mm}(r, z). \quad (8)$$

In what follows, we will compute the halo correlation functions for dark matter haloes in mass bins and compare with those measured from N-body simulations.

2.2 N-body simulations

Our study mainly uses two cosmological dark matter N-body simulations, the MS-W7 simulation (Guo et al. 2013; Pike et al. 2014) and the Millennium-XXL or MXXL simulation (Angulo et al. 2012). The MS-W7 simulation uses a cubic computational box of comoving length 500 h^{-1} Mpc with 2160^3 particles of mass $8.61 \times 10^8\,{\rm M}_\odot$. This is used to probe the clustering of haloes at $z = 3$, 4 and 5. It adopts a flat ΛCDM background cosmology, which is in agreement with the WMAP7 results (Larson et al. 2011), with $h = 0.704$, $\Omega_{\rm b} = 0.0455$, $\Omega_{\rm c} = 0.2265$, $\Omega_\nu = 0.0$, $\sigma_8 = 0.81$ and $n_{\rm s} = 0.967$.

The MXXL extends the previous Millennium and Millennium-II simulations (Springel et al. 2005; Boylan-Kolchin et al. 2009) and follows the evolution of 6720^3 dark matter particles inside a cubic box of length 3000 h^{-1} Mpc. The particle mass is $8.46 \times 10^9\,{\rm M}_\odot$. This simulation adopts a ΛCDM cosmology with the same cosmological parameters as the previous Millennium simulations. Accordingly, $h = 0.73$, $\Omega_{\rm b} = 0.045$, $\Omega_{\rm c} = 0.205$, $\Omega_\nu = 0.0$, $\sigma_8 = 0.9$ and $n_{\rm s} = 1.0$. The MXXL haloes are used to investigate the clustering at $z = 0$, 1, 2 and 3. We also compare the results obtained using MXXL simulation at $z = 3$ with those obtained using the Millennium simulation at the same redshift, which has a box of 500 h^{-1} Mpc.

In both simulations, groups of more than 20 particles are identified as dark matter haloes using a friends-of-friends algorithm [FOF(0.2)] with linking parameter equal to 0.2 of the mean particle separation (Davis et al. 1985). The halo mass functions from these simulations are well described by the fitting function of Jenkins et al. (2001) over a wide range of halo masses and to an accuracy better than 10 per cent.

The two-point correlation functions of dark matter haloes and dark matter particles from the simulations are computed by counting the number of pairs as a function of the separation, r, relative to that of a random distribution and is given by

$$\xi^{\rm sim}(r) = \frac{N^{\rm p}(r)}{N^{\rm p}_{ran}(r)} - 1, \quad (9)$$

where $N_{\rm p}(r)$ is the total number of pairs in the simulation separated by a distance r to $r + \delta r$ and $N^{\rm p}_{ran}(r)$ is the total number of pairs.

As mentioned above, in this paper, we focus on the clustering of rare dark matter haloes on quasi-linear scales in the redshift range 0–5. Therefore, we consider only those haloes with a peak height $\nu(M, z) > 1$. At $z \sim 0$, the typical masses of these haloes range between 10^{13} and $10^{15}\,{\rm M}_\odot$ and therefore they correspond to poor galaxy groups and clusters. On the other hand, for $z \geq 2$, the masses of rare haloes range from 10^{10} to $10^{13}\,{\rm M}_\odot$. As we see later, the scale dependence of the halo bias due to nonlinear clustering is much more significant at higher redshifts ($z = 2$–5) than it is at lower redshifts. Therefore, we first address the issue of the nonlinear clustering of high redshift dark matter haloes on quasi-linear scales and then its evolution in the low redshift universe.

2.3 Comparing simulations and linear bias models

We first show that the clustering strength of high-z, rare dark matter haloes on quasi-linear scales differs significantly from the predictions of the linear bias model by comparing with the spatial correlation functions estimated from N-body simulations. In the top panels of Fig. 1, the halo correlation functions estimated from simulations ($\xi^{\rm sim}_{\rm hh}(M, r, z)$) are shown at $z = 2$–5 for haloes in the mass range 9×10^{10}–$10^{11}\,h^{-1}\,{\rm M}_\odot$ (black circles) and $2 \times 10^{12} - 4 \times 10^{12}\,h^{-1}\,{\rm M}_\odot$ (red triangles). We note that, these haloes respectively host typical Lyman-alpha emitters (LAEs) and Lyman-break galaxies (LBGs) in the same redshift range (Jose, Srianand & Subramanian 2013a; Jose et al. 2013b) and are rare haloes, collapsing from 2σ–3σ fluctuations ($\nu(M, z) \sim 2$–3). On small scales the correlation functions drop to -1 due to halo exclusion. These scales correspond to the typical virial radius of haloes in the given mass bin.

Also shown in the top panels of Fig. 1 are the correlation functions, $\xi_{\rm hh}(M, r, z)$, predicted by equation (8) for the same cosmological parameters as used in the simulations. The correlation functions are computed for haloes in the same mass bins used to estimate $\xi^{\rm sim}_{\rm hh}(M, r, z)$. Fig. 1 clearly shows that $\xi^{\rm sim}_{\rm hh}(r, z)$ and $\xi_{\rm hh}(r, z)$ agree well with each other on large scales ($r \gtrsim 10$–$15\,h^{-1}$ Mpc). However, on quasi-linear scales ($r \sim 0.5$–$10\ h^{-1}$ Mpc), $\xi^{\rm sim}_{\rm hh}(r, z)$ determined from the simulations shows an excess compared to $\xi_{\rm hh}(r, z)$ computed using equation (8).

To understand the degree of this deviation more clearly, we have plotted in the bottom panels of Fig. 1 the ratio of the dark matter halo correlation functions measured from simulations to that computed from the linear bias model (i.e. $\xi^{\rm sim}_{\rm hh}(r, z)/\xi_{\rm hh}(r, z)$) for each mass bin. It is clear from the figure that, on quasi-linear scales, the predictions of the scale-independent bias model are insufficient to explain the halo correlation functions measured directly from the simulations. For example, the massive haloes at the highest redshift ($2 \times 10^{12} \leq M/{\rm M}_\odot \leq 4 \times 10^{12}$ at $z = 5$) show clustering in the simulations that is sometimes larger by a factor as large as ~ 20 at $1 \leq r \leq 2$ Mpc h^{-1}, compared to the linear bias model predictions. On the other hand, at lower redshifts and for less massive haloes ($9 \times 10^{10} \leq M/{\rm M}_\odot \leq 10^{11}$ at $z = 3$), the clustering excess is only a factor of 2–3 at $r \sim 0.5$ Mpc h^{-1}. Furthermore, the deviation between $\xi^{\rm sim}_{\rm hh}(r, z)$ and $\xi_{\rm hh}(r, z)$ increases with the redshift and mass of dark matter haloes. Overall we conclude that the halo bias of high redshift dark matter haloes is strongly scale dependent on quasi-linear scales and the scale dependence increases with the rarity of the haloes.

Earlier studies focused on the nonlinear bias of haloes at the present epoch (Hamana et al. 2001; Diaferio et al. 2003; Tinker et al. 2005) or at redshifts before reionization (Reed et al. 2009). The scale dependence of the nonlinear bias in the fitting functions provided by Hamana et al. (2001), Diaferio et al. (2003), Tinker et al. (2005) is too weak to explain the clustering of haloes at the redshifts, masses and scales of interest here. The fitting function of Reed et al. (2009) has a stronger scale dependence and describes the nonlinear clustering of high redshift MS-W7 haloes correctly. However, as we see later, their results are not consistent with the bias measured from the MXXL simulation and also at lower redshifts ($z = 0$–2). Therefore, nonlinear clustering of rare haloes on

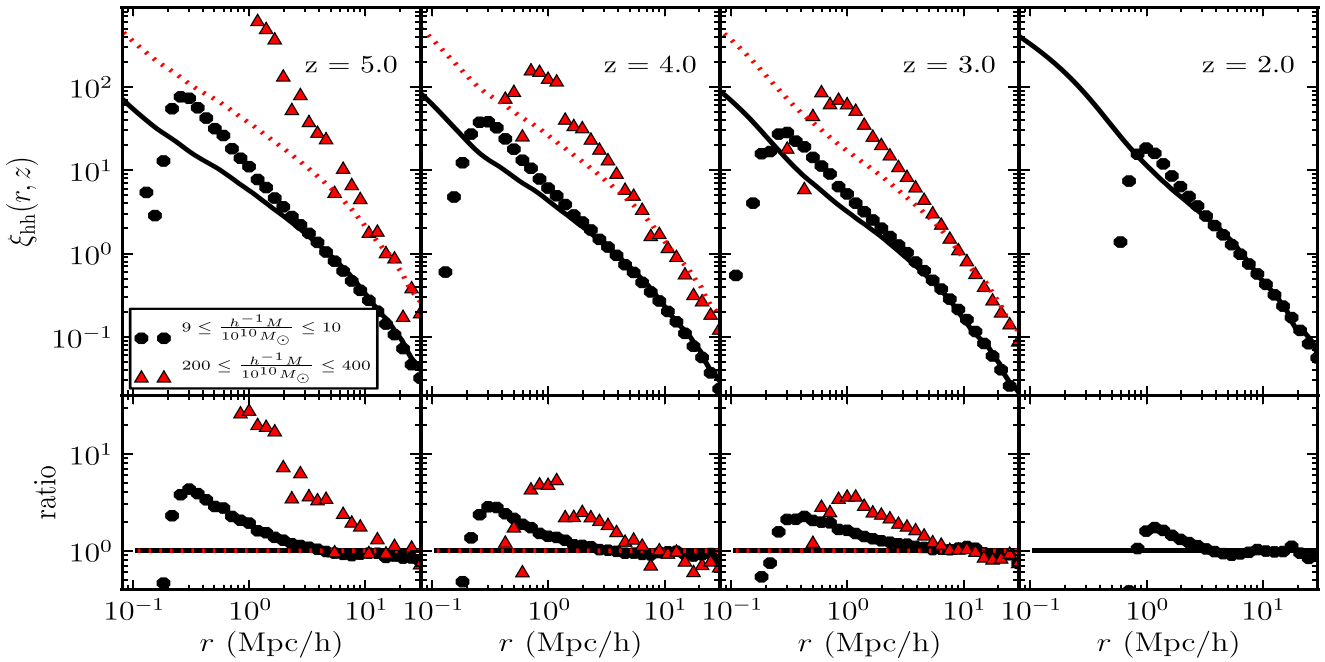

Figure 1. Upper panels : the two-point correlation functions of dark matter haloes in the mass range $\sim 10^{11} - 5 \times 10^{12}\,\mathrm{M}_\odot$ at various redshifts as labelled. The points (triangles and circles) are measured from *N*-body simulations and the curves (solid and dotted) are analytic predictions using the linear bias approximation with the same cosmological parameters as used in the simulations. The results at $z = 2$ are from the MXXL simulation and those at other redshifts are from the MS-W7 simulation. Bottom panels: the ratio of the correlation functions measured from simulations to those computed analytically.

quasi-linear scales has not been satisfactorily addressed and thus warrants further investigation.

3 THE SCALE-DEPENDENT, NONLINEAR HALO BIAS

3.1 The measured bias

We have shown in the previous section that, on quasi-linear scales, high-z dark matter haloes collapsing from 2σ–3σ fluctuations cluster more strongly than the predictions of the linear bias model. Therefore, to understand the clustering of these rare haloes, one has to invoke a scale-dependent, nonlinear bias. For this, we first define a nonlinear, scale-dependent halo bias of dark matter haloes at any redshift as (Scannapieco & Barkana 2002; Reed et al. 2009)

$$b_{\rm nl}(r, M, z) = \sqrt{\frac{\xi^{\rm sim}_{\rm hh}(r, z)}{\xi^{\rm sim}_{\rm mm}(r, z)}}. \quad (10)$$

Here, $\xi^{\rm sim}_{\rm mm}(r, z)$ is the nonlinear dark matter correlation function computed directly from the simulations using equation (9). The function $b(r, M, z)$ is thus expected to be independent of r on large scales.

We note that there are alternative definitions of the halo bias in Fourier space and also as the ratio of the halo-matter cross-correlation function to the matter correlation function (e.g. Tinker et al. 2010; Manera & Gaztañaga 2011). The choice of a particular definition of the halo bias can in principle introduce a scale dependence in the bias measured from the simulations (Baumann et al. 2013). This scale dependence introduces a few per cent difference between the measured bias that is defined by equation (10) and those defined by other bias definitions (Smith & Marian 2011; Pollack, Smith & Porciani 2012). This effect is much weaker compared to the strong scale dependence of the halo bias presented in this work and hence will be neglected. We also note that $b_{\rm nl}(r, M, z)$, defined by equation (10), encapsulates the scale dependence of the halo bias due to the nonlinear higher order correlations of the matter distribution and also due to the scale dependence of the linear halo bias. Thus, one can directly use $b_{\rm nl}(r, M, z)$ to compute the $\xi_{\rm hh}$ at any given scale in real space using equation (5) with minimum ambiguities, which is our primary goal.

In the previous section, we estimated the clustering of haloes in different mass bins. However, it would be more useful if the nonlinear bias could be calculated from the dark matter power spectrum. One could then hope to apply our results in more general contexts. Furthermore, as discussed in the previous section, we first focus on high redshift haloes. Therefore, we measured the scale-dependent halo bias $[b_{\rm nl}(r, M, z)]$ of dark matter haloes from the MS-W7, MXXL and Millennium simulations in bins of peak height, $\nu(M, z)$, in the redshift range 2–5.

First, we briefly discuss the effects of resolution and the halo exclusion effect on the estimated nonlinear bias by comparing results obtained using MXXL and Millennium haloes at $z = 3$. As discussed before, these simulations have the same set of cosmological parameters, but different mass resolutions and volumes. In Fig. 2, we have plotted the nonlinear and scale-dependent bias at $z = 3$ for haloes (in a given ν bin) from the MXXL and Millennium simulations. Also shown by the vertical line, is the length-scale corresponding to twice the virial radius of the most massive halo in each sample.

We first note that in Fig. 2, the scale-dependent bias at $z = 3$ is expressed as a function of $\xi^{\rm sim}_{\rm mm}(r, z)$ at the same redshift. This choice has been made in several analytic and numerical studies probing the clustering of dark matter haloes on quasi-linear scales (Hamana et al. 2001; Scannapieco & Barkana 2002; Diaferio et al. 2003; Tinker et al. 2005; Reed et al. 2009; van den Bosch et al. 2013). These studies present the scale-dependent bias, $b_{\rm nl}(r, M, z)$ as a function of the nonlinear dark matter correlation function, $\xi^{\rm sim}_{\rm mm}(r, z)$

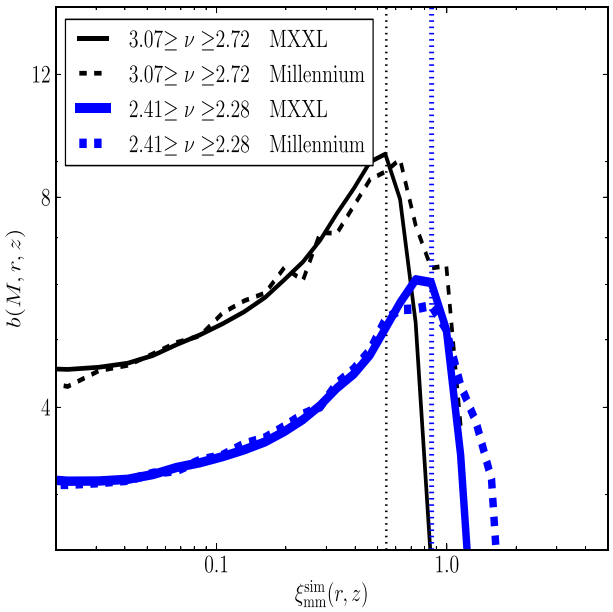

Figure 2. The halo bias $b(r, M, z) = \sqrt{\xi^{\rm sim}_{\rm hh}(r, z)/\xi^{\rm sim}_{\rm mm}(r, z)}$ computed at $z = 3$ using Millennium and MXXL haloes in $\nu(M, z)$ bins, as indicated by the label. The thick (blue) and thin (black) lines respectively correspond to haloes with $2.41 \geq \nu \geq 2.28$ and $3.07 \geq \nu \geq 2.72$. The thick (blue) and thin (black) vertical lines indicate scales corresponding to twice the virial radius of the most massive halo in each sample.

at the same redshift. In what follows, we adopt this approach and express $b_{\rm nl}(r, M, z)$ as a function of $\xi^{\rm sim}_{\rm mm}(r, z)$. In this approach, the scale-dependent bias can be thought of as a function of the nonlinear dark matter power spectrum, since the matter correlation function is the Fourier transform of the nonlinear dark matter power spectrum.

It is clear from Fig. 2 that the halo bias estimated from the two simulations agree well with one another on scales larger than twice the virial radius of the most massive halo in the sample. However, on smaller scales, the estimated halo bias is different between the two simulations. Since both simulations use the same set of cosmological parameters, this could be due to the difference in mass resolution between the simulations. We also note that, on the largest scales [$\xi^{\rm sim}_{\rm mm}(r, z) < 0.05$], the bias is approximately a constant. On smaller scales, the nonlinear bias increases with decreasing scale (increasing $\xi^{\rm sim}_{\rm mm}$) and reaches a maximum value around the scale corresponding to twice the virial radius of the most massive halo in the sample. On smaller scales than this, the halo bias drops to 0. This suggest that, while probing the clustering of a sample of haloes, the halo exclusion effect is important on scales smaller than twice the virial radius of the most massive halo in the sample. Because of these effects due to the resolution and halo exclusion, our further discussion and analysis will consider the clustering of a sample of haloes only on scales larger than twice the virial radius of the most massive halo in that sample.

We now present our estimates of the nonlinear bias from different simulations at various redshifts in Fig. 3 as a function of $\xi^{\rm sim}_{\rm mm}(r, z)$. The results measured from the MXXL simulation at $z = 2$ are shown by solid black lines and at $z = 3$ are shown using red circles. All the other curves at $z = 3$–5 are estimates of $b_{\rm nl}(r, M, z)$ from the MS-W7 simulation. Each panel corresponds to a different bin of $\nu(M, z)$ (see labels). We again emphasize that $b_{\rm nl}(M, r, z)$ at a given redshift is plotted against $\xi^{\rm sim}_{\rm mm}(r, z)$ at the same redshift.

We first note that, on scales corresponding to $\xi^{\rm sim}_{\rm mm} \lesssim 0.1$, $b_{\rm nl}(r, M, z)$ measured from the MS-W7 and MXXL simulations agree well with each other. On smaller scales, the estimated bias is different for the two simulations. The halo bias measured from the MXXL simulation drops to zero on larger scales compared to the bias estimated from the MS-W7 simulation. This is because, for haloes in a given ν bin, the masses and virial radii of MXXL haloes are larger than those of MS-W7 haloes.

3.2 A model for the halo bias

As discussed before, $b_{\rm nl}(r, M, z)$ at different redshifts is fairly constant for $\xi^{\rm sim}_{\rm mm} \lesssim 0.05$. These scales typically correspond to comoving length-scales greater than $10\,h^{-1}$ Mpc. Thus on such large scales, the expression for the nonlinear bias reverts back to the usual scale-independent large scale bias, which is only a function of the peak height ν alone. Therefore, one can write

$$b_{\rm nl}(r, M, z) = \gamma(r, M, z) b(\nu), \tag{11}$$

where $b(\nu)$ is the large scale bias. Here the nonlinear bias, $b_{\rm nl}(r, M, z)$, is written as the product of a scale-dependent function, $\gamma(r, M, z)$, and the large scale bias. The scale-dependent function $\gamma(r, M, z)$ is thus expected to be close to unity on large scales.

To understand the evolution of the nonlinear bias of rare haloes with redshift, one has to calibrate the expressions for the large scale linear bias $b(\nu)$ and scale-dependent function $\gamma(r, M, z)$. In what follows, we first obtain a fitting function for $b(\nu)$ and then constrain the functional form of $\gamma(r, M, z)$.

3.3 The large scale bias

To estimate $b(\nu)$, we measured the correlation functions of dark matter haloes in different $\nu(M, z)$ bins in the redshift range 0–5. These ν-bins are given in column 1 of Table 1. Also given in the table are the average peak height, $\nu_{\rm av}$ and average mass of haloes, $M_{\rm av}$, in these bins at each redshift. The average peak height is given by $\nu_{\rm av} = \delta_c/\sigma_{\rm av}$, where $\sigma_{\rm av}$ is computed as

$$\sigma^2_{\rm av}(z) = \frac{\int {\rm d}M n(M, z)\sigma^2(M, z)}{\int {\rm d}M n(M, z)}. \tag{12}$$

We define the large scale bias, $b(\nu)$, as the average bias of haloes that are separated by $10 \leq r \leq 25$ Mpc h^{-1}, i.e.

$$b(\nu) = \sqrt{\frac{\int_{10}^{25} {\rm d}r r^2 \xi_{\rm hh}(\nu, \xi^{\rm sim}_{\rm mm}(r))}{\int_{10}^{25} {\rm d}r r^2 \xi^{\rm sim}_{\rm mm}(r)}}. \tag{13}$$

We then obtain a fitting function for $b(\nu)$ by refitting the free parameters of equation (4) to the $b(\nu)$ measured from the simulations using equation (13). The best-fitting parameters are estimated to be $A = 1.0$, $a = 0.36$, $B = -1.156$, $b = 2.18$, $C = -0.749$ and $c = 2.18$, treating all bias values with equal weight.

In Fig. 4, our fit (black solid line) for $b(\nu)$ is overplotted with the symbols measured directly from the simulation at different redshifts. The data points at $z = 0$–2 are measured from the MXXL simulation and those at $z = 3$–5 are obtained from MS-W7 simulation. It is clear from Fig. 4 that our fitting function for $b(\nu)$ agrees very well with the measurements from the simulations. In fact, we find that, the overall agreement between the simulation results and the fitting function is within 3 per cent. Also shown in Fig. 4 are the fitting functions for halo bias from Sheth & Tormen (1999) (ST, red dotted curve) and Tinker et al. (2010) (Tinker, blue dashed curve). One can see from the figure that when $\nu(M) \lesssim 2$, our formula compares well with

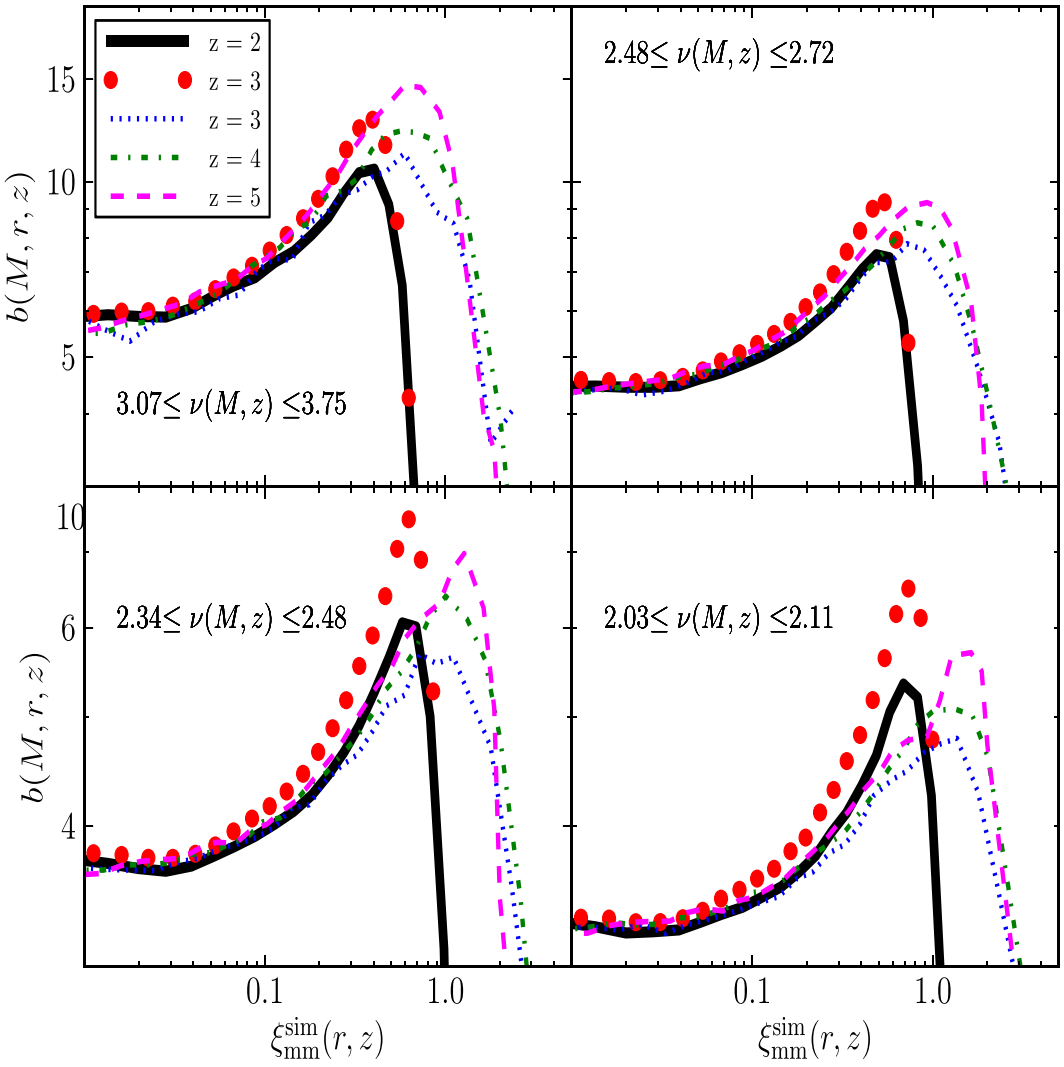

Figure 3. The halo bias $b(r, M, z) = \sqrt{\xi^{\rm sim}_{\rm hh}(r, z)/\xi^{\rm sim}_{\rm mm}(r, z)}$ plotted as a function of $\xi^{\rm sim}_{\rm mm}(r, z)$ in the redshift range 2–5. Each panel shows the $b(r, M, z)$ of haloes in $\nu(M, z)$ bins, as indicated by the label. The results obtained from the MXXL simulation are shown by the solid black lines ($z = 2$) and red circles ($z = 3$) whereas other curves corresponds to the results from the MS-W7 simulation.

these two fitting functions (particularly with the Tinker formula). However, for larger values of $\nu(M)$, the ST formula predicts lower bias values and Tinker formula gives slightly larger bias values compared with our formula for halo bias. Thus for rarer haloes with $\nu \geq 2$, our analysis predicts a slightly lower value for the large scale bias compared to the Tinker formula. However, we also note that Tinker et al. (2010) use the spherical overdensity (SO) algorithm (Tinker et al. 2008) to identify haloes, which is different from the FOF(0.2) algorithm used in this work. Such a difference in the bias of haloes identified by these two algorithms has already been noted by Tinker et al. (2008, 2010). Further, the simulations used by Tinker et al. (2010) span a wider range of cosmological parameters than used in this work. This could also account for the difference between the estimated large scale halo bias.

3.4 The scale dependence of halo bias

Having obtained the expression for the large scale ($r \geq 10$ Mpc h^{-1}) bias of rare haloes in the redshift range 0–5, we now wish to calibrate the scale dependence $\gamma(M, r, z)$ of $b(r, M, z)$ on quasi-linear scales. We first concentrate on the expression for $\gamma(M, r, z)$ of haloes in the redshift range 2–5. This is because, as we shall see later, $\gamma(M, r, z)$ probably has an explicit dependence on the effective matter density $\Omega_{\rm m}(z)$ of the universe as a function of redshift. We expect to separate out this dependence by focusing on high redshifts ($z \geq 2$) where $\Omega_{\rm m}(z) \approx 1$.

It is clear from Fig. 3 that the scale-dependent, nonlinear bias of haloes (from the MS-W7 simulation) of a given $\nu(M, z)$ as function of $\xi^{\rm sim}_{\rm mm}(r, z)$ and at $z = 3$–5, agree fairly well with each other. In fact, in this case, the agreement between estimates of $b(r, M, z)$ at different redshifts is better than 10 per cent on quasi-linear scales ($r \leq 15\,h^{-1}$ Mpc). However, Fig. 3 shows that the scale dependence $b(r, M, z)$ of MXXL haloes for the same $\nu(M, z)$ at $z = 2$ and 3 (which is also expressed as function of $\xi^{\rm sim}_{\rm mm}(r, z)$) is quite different from that of MS-W7 haloes at higher redshift. Thus, $\gamma(M, r, z)$, which accounts for the scale dependence of $b(r, M, z)$, cannot be described as a function of just two variables, $\xi^{\rm sim}_{\rm mm}(r, z)$ and $\nu(M, z)$. This suggests that the nonlinear bias on quasi-linear scales is not a simple function of the dark matter power spectrum and any fitting function should be a function of other parameters.

Such an explicit dependence of the halo bias on parameters other than the dark matter power spectrum has been discussed in

Table 1. Column 1: the $\nu(M, z)$ bins of haloes used to calibrate the nonlinear bias. Column 2: the corresponding average peak height, $\nu_{\rm av}$. Other columns give the average mass, $M_{\rm av}$, of haloes in the sample at the given redshift. If $M_{\rm av}$ is not given, then the $\nu(M, z)$ bin is not used in our analysis. Columns 3–6 results are for MXXL haloes, columns 7–9 are for MS-W7 haloes whereas column 10 refers to Millennium haloes.

$(\nu_{\rm min}, \nu_{\rm max})$	$\nu_{\rm av}$	$M_{\rm av}/{\rm M}_\odot$							
		MXXL haloes				MS-W7 haloes			Millennium haloes
		$z=0$	$z=1$	$z=2$	$z=3$	$z=3$	$z=4$	$z=5$	$z=3$
(3.37, 4.21)	3.77	1.9×10^{15}	3.0×10^{14}	6.1×10^{13}	1.5×10^{13}	8.0×10^{12}	2.7×10^{12}	7.4×10^{11}	1.5×10^{13}
(3.07, 3.37)	3.22	1.2×10^{15}	1.8×10^{14}	3.3×10^{13}	7.7×10^{12}	3.9×10^{12}	1.2×10^{12}	3.1×10^{11}	7.7×10^{12}
(2.81, 3.07)	2.93	8.9×10^{14}	1.2×10^{14}	2.1×10^{13}	4.5×10^{12}	2.2×10^{12}	6.5×10^{11}	1.6×10^{11}	4.5×10^{12}
(2.59, 2.81)	2.70	6.5×10^{14}	8.2×10^{13}	1.3×10^{13}	2.7×10^{12}	1.3×10^{12}	3.6×10^{11}	8.0×10^{10}	2.7×10^{12}
(2.44, 2.59)	2.52	5.0×10^{14}	5.9×10^{13}	9.2×10^{12}	1.8×10^{12}	8.0×10^{11}	2.1×10^{11}	–	1.8×10^{12}
(2.28, 2.41)	2.34	3.7×10^{14}	4.2×10^{13}	6.0×10^{12}	1.1×10^{12}	4.8×10^{11}	1.2×10^{11}	–	1.1×10^{12}
(2.19, 2.28)	2.23	3.0×10^{14}	3.3×10^{13}	4.6×10^{12}	–	3.4×10^{11}	8.2×10^{10}	–	8.0×10^{11}
(2.11, 2.19)	2.15	2.6×10^{14}	2.7×10^{13}	3.6×10^{12}	–	2.5×10^{11}	5.9×10^{10}	–	6.1×10^{11}
(2.03, 2.11)	2.07	2.2×10^{14}	2.2×10^{13}	2.9×10^{12}	–	1.9×10^{11}	–	–	4.7×10^{11}
(1.96, 2.03)	2.00	1.9×10^{14}	1.8×10^{13}	2.3×10^{12}	–	1.4×10^{11}	–	–	3.6×10^{11}
(1.87, 1.92)	1.89	1.5×10^{14}	1.4×10^{13}	1.6×10^{12}	–	9.2×10^{10}	–	–	2.5×10^{11}
(1.77, 1.81)	1.79	1.2×10^{14}	1.0×10^{13}	1.1×10^{12}	–	5.8×10^{10}	–	–	1.6×10^{11}
(1.69, 1.72)	1.70	9.2×10^{13}	7.5×10^{12}	–	–	–	–	–	1.1×10^{11}
(1.53, 1.56)	1.55	5.8×10^{13}	4.2×10^{12}	–	–	–	–	–	4.9×10^{10}
(1.30, 1.32)	1.31	2.5×10^{13}	1.5×10^{12}	–	–	–	–	–	–
(1.12, 1.14)	1.13	1.1×10^{13}	–	–	–	–	–	–	–

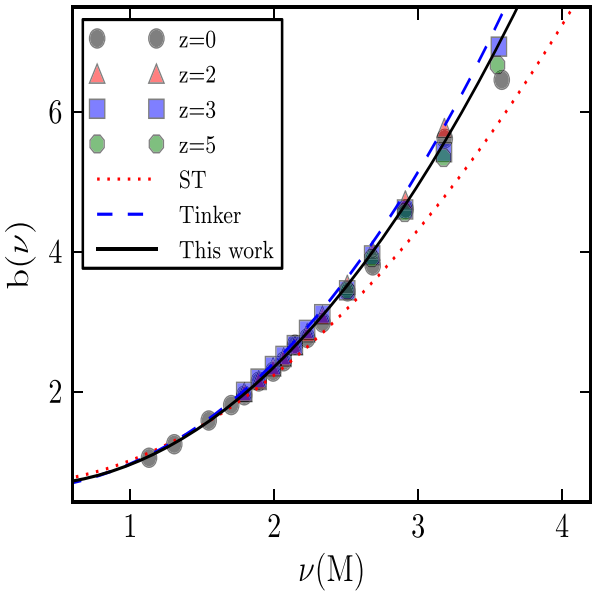

Figure 4. Our fit to equation (4) for the large scale linear halo bias (solid black curve) along with the simulation measurements (symbols) at various redshifts. The points for $z = 0$ and 2 are measured from the MXXL simulation and those at $z = 3$ and 5 are obtained from the MS-W7 simulation. The red dotted and blue dashed curves are the fitting functions of the linear halo bias given by Sheth & Tormen (1999) (ST) and Tinker et al. (2010) (Tinker), respectively.

several analytical studies (Blanton et al. 1999; Matsubara 1999; Iliev et al. 2003; Sheth & Tormen 2004; Gao, Springel & White 2005a; Jeong & Komatsu 2009; McDonald & Roy 2009; Lazeyras, Musso & Desjacques 2016). These studies point out that one may potentially require an infinite number of parameters to express the scale-dependent bias. On the other hand, most of the available fits to the results of N-body simulations present the scale-dependent halo bias as a universal function of the dark matter power spectrum (Hamana et al. 2001; Diaferio et al. 2003; Cen et al. 2004; Gao et al. 2005b; Tinker et al. 2005; Reed et al. 2009; Desjacques et al. 2010). We will now investigate whether the scale dependence of the halo bias measured from the simulations can be expressed as a function of additional parameters along with $\xi^{\rm sim}_{\rm mm}(r, z)$ and $\nu(M, z)$.

We find that adding one more parameter can account for all the simulation results in the redshift range 2–5. That is, $\gamma(M, r, z)$ at $2 \le z \le 5$ can be expressed, to sufficient accuracy, as function of three variables, $\nu(M, z)$, $\xi^{\rm sim}_{\rm mm}(r, z)$ and $\alpha_{\rm m}(z)$, an effective power-law index of $\sigma(M, z)$. This effective power-law index is defined as

$$\alpha_{\rm m}(z) = \frac{\log(1.686)}{\log[M_{nl}(z)/M_{col}(z)]}, \tag{14}$$

where the nonlinear mass scale, $M_{\rm nl}(z)$, and the collapse mass scale, $M_{\rm col}(z)$, at any redshift are masses at which the peak heights are, respectively, 1.686 and 1. The parameter $\alpha_{\rm m}(z)$ can be thought of as an effective power-law index of $\sigma(M, z)$ in the mass range from the collapse to the nonlinear mass scale (see Appendix A for more details). The dependence of $\gamma(M, r, z)$ on $\alpha_{\rm m}(z)$ can be tentatively understood from Fig. 5, where we have plotted this ratio as a function of z. The blue triangles at $z = 3$–5 are obtained for the MS-W7 and the red circles at lower redshifts are for the MXXL cosmological parameters. The figure clearly shows that $\alpha_{\rm m}(z)$ is nearly constant in the redshift range $3 - 5$ for the MS-W7 cosmology. However, at $z = 2$ where the MXXL cosmology is used, $\alpha_{\rm m}(z)$ is larger. Such a difference is perhaps related to the departure from the universal nature of nonlinear bias as a function of $\nu(M, z)$ and $\xi^{\rm sim}_{\rm mm}(r, z)$. Motivated by this, we further investigated whether $\gamma(M, r, z)$ can be expressed as a function of $\nu(M, z)$, $\xi^{\rm sim}_{\rm mm}(r, z)$ and $\alpha_{\rm m}(z)$ and we find that, it is indeed possible to obtain a good fit for high-σ haloes ($\nu > 1$). The resulting fitting function is given by

$$\begin{aligned}\gamma(&\xi^{\rm sim}_{\rm mm}, \nu, \alpha_{\rm m}) \\ &= \left(1 + K_0(1 + k_3/\alpha_{\rm m}) \log\left(1 + \xi^{{\rm sim}k_1}_{\rm mm}\right) \nu^{k_2}\right) \\ &\quad \times \left(1 + L_0(1 + l_3/\alpha_m) \log\left(1 + \xi^{{\rm sim}l_1}_{\rm mm}\right) \nu^{l_2}\right).\end{aligned} \tag{15}$$

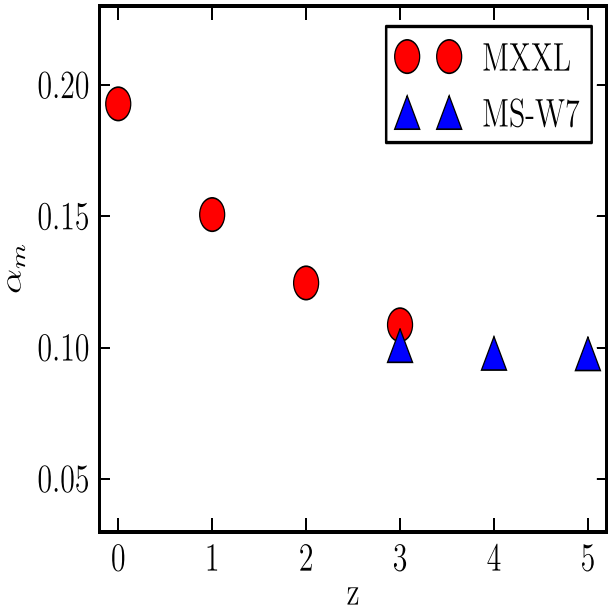

Figure 5. The effective power-law index, $\alpha_{\rm m}$, (equation (14)) is plotted as a function of redshift. The blue triangles and red circles correspond to the values obtained for the MS-W7 and the MXXL cosmology, respectively.

The free parameters are estimated to be $K_0 = -0.0697$, $k_1 = 1.1682$, $k_2 = 4.7577$, $k_3 = -0.1561$, $L_0 = 5.1447$, $l_1 = 1.4023$, $l_2 = 0.5823$ and $l_3 = -0.1030$. In fitting equation (15), we have used the nonlinear bias estimated from simulations for all $\nu(M, z)$ bins in redshift range $z = 2$–5 given in Table 1. For fitting $\gamma(\xi^{\rm sim}_{\rm mm}, \nu, \alpha_{\rm m})$, we considered halo correlation functions only on scales larger than twice the virial radius of the most massive halo in the sample. Moreover, we have restricted our analysis to $r \leq 30h^{-1}$ Mpc.

It is also important to note from Table 1 that the masses of the haloes used in our analysis range typically from 5×10^{10} to $5 \times 10^{13} h^{-1}\,{\rm M}_\odot$. Thus, the high-$\sigma$ haloes of interest are those expected to host galaxies in the redshift range 2–5.

The expression for $\gamma(\xi^{\rm sim}_{\rm mm}, \nu)$ in equation (15) is plotted (solid line) in Fig. 6 at different redshifts as a function of $\xi^{\rm sim}_{\rm mm}(r)$ at that redshift and for different values of $\nu(M)$. In Fig. 6, the results shown at $z = 2$ are from the MXXL simulation and those at other redshifts are from the MS-W7 simulation. From Fig. 6, it is clear that the parametrization of $\gamma(\xi^{\rm sim}_{\rm mm}, \nu, \sigma_{\rm eff})$ using equation (15) fits the whole range of data measured directly from the simulations very well. In particular, we note that our fit is consistent with the results from simulations to within an overall accuracy of 4 per cent. This suggests that, it is indeed possible to find a fitting function for the scale dependence of the nonlinear bias in the redshift range 2–5, through $\xi^{\rm sim}_{\rm mm}$, ν and $\alpha_{\rm m}$.

In Fig. 6, we have also plotted in dotted lines, the fitting function for γ given by Reed et al. (2009). These authors parametrized the scale dependence as a function of the large scale bias $b(\nu)$ and $\sigma(r, z)$ as

$$\gamma(b(\nu), \sigma(r, z)) = [1 + 0.03b^3(\nu)\sigma^2(r, z)]. \quad (16)$$

It is clear from Fig. 6 that the Reed et al. (2009) fit compares reasonably well with results from the MXXL and MS-W7 simulations at $z = 3$–5, especially at $z = 5$. However, their formula is not quite consistent with the MXXL simulation results at $z = 2$. This is expected, since the Reed et al. (2009) expression for nonlinear bias of a halo of mass M at a scale r depends only on the dark matter power spectrum through the *rms* linear density fluctuations on the mass scale M and length-scale r. As noted before, such a simple dependence cannot accurately account for the scale dependence of the nonlinear bias seen from simulations.

3.5 The evolution of $\gamma(M, r, z)$ to low redshifts

Having obtained a fitting function for $\gamma(r, M, z)$ for high-z haloes in the entire redshift range 2–5, we now include low-z data to probe the evolution of the scale dependence of nonlinear bias from $z = 0$–5. We note from Table 1 that, at $z = 0$ and 1, the masses of the rare dark matter haloes used in our study ranges from 10^{12} to $10^{15} h^{-1}\,{\rm M}_\odot$; correspondingly they host galaxies as well as groups and clusters.

In Fig. 7, we show $\gamma(r, M, z)$ estimated from the simulations (symbols) over the full redshift range. The data at $z = 3$–5 are measured from MS-W7 and those at $z = 0$–2 are from the MXXL simulation. It is clear from the figure that at lower redshifts ($z = 0$ and 1) the scale dependence of the nonlinear bias is rather weaker compared to other redshifts. Such a weak scale dependence of halo bias on quasi-linear scales at lower redshifts ($z = 1$) can be found also in the analytic work of Scannapieco & Barkana (2002). In particular, at $z = 0$, the halo bias increases by only ∼10 per cent on quasi-linear scales even for the most massive and hence rarest haloes at that redshift.

It turns out that one can obtain a fit for the nonlinear bias which extends to redshift 0 by adding an additional parameter, $\Omega_{\rm m}(z)$, the matter density of the universe at a given redshift as follows:

$$\Omega_{\rm m}(z) = \frac{\Omega_{\rm m}(1+z)^3}{\Omega_{\rm m}(1+z)^3 + \Omega_\Lambda}. \quad (17)$$

Thus, the evolution of $\gamma(r, M, z)$ in the redshift range 0–5 can be expressed as a function of four variables, $\Omega_{\rm m}(z)$, $\nu(M, z)$, $\xi^{\rm sim}_{\rm mm}(r, z)$ and $\alpha_{\rm m}(z)$. In particular, we obtained a fitting function for $\gamma(r, M, z)$ using the nonlinear bias estimated from simulations for haloes in bins of $\nu(M, z)$ in the redshift range $z = 0$–5 given in Table 1. As before, we have used the correlation functions only on scales larger than twice the virial radius of the biggest halo in the sample and smaller than 30 Mpc h^{-1} for the analysis. The resulting fitting function is given by:

$$\begin{aligned}\gamma(&\xi^{\rm sim}_{\rm mm}, \nu, \alpha_{\rm m}, \Omega_{\rm m}(z)) \\ &= \left(1 + K_0(1 + k_3/\alpha_{\rm m})(\Omega_{\rm m}(z))^{k_4} \log\left(1 + \xi^{{\rm sim}k_1}_{\rm mm}\right)\nu^{k_2}\right) \\ &\quad \times \left(1 + L_0(1 + l_3/\alpha_{\rm m})(\Omega_{\rm m}(z))^{l_4} \log\left(1 + \xi^{{\rm sim}l_1}_{\rm mm}\right)\nu^{l_2}\right). \quad (18)\end{aligned}$$

Here $K_0 = 0.1699$, $k_1 = 1.194$, $k_2 = 4.311$, $k_3 = -0.0348$, $k_4 = 17.8283$, $L_0 = 2.9138$, $l_1 = 1.3502$, $l_2 = 1.9733$, $l_3 = -0.1029$ and $l_4 = 3.1731$. The fitting function in equation (18) is plotted as solid lines in Fig. 7 along with data points measured from simulations. Our fit is in remarkable agreement with data from all the simulations over the entire range of redshifts from 0 to 5, peak heights and length-scales. The overall agreement of this fit with the data from the simulations is found to be better than 4 per cent.

3.6 Halo clustering as a function of the linear matter correlation function

We have, so far, presented a model for the nonlinear clustering of dark matter haloes as a function of the nonlinear dark matter correlation function, $\xi^{\rm sim}_{\rm mm}(r, z)$, measured from the simulations. In this

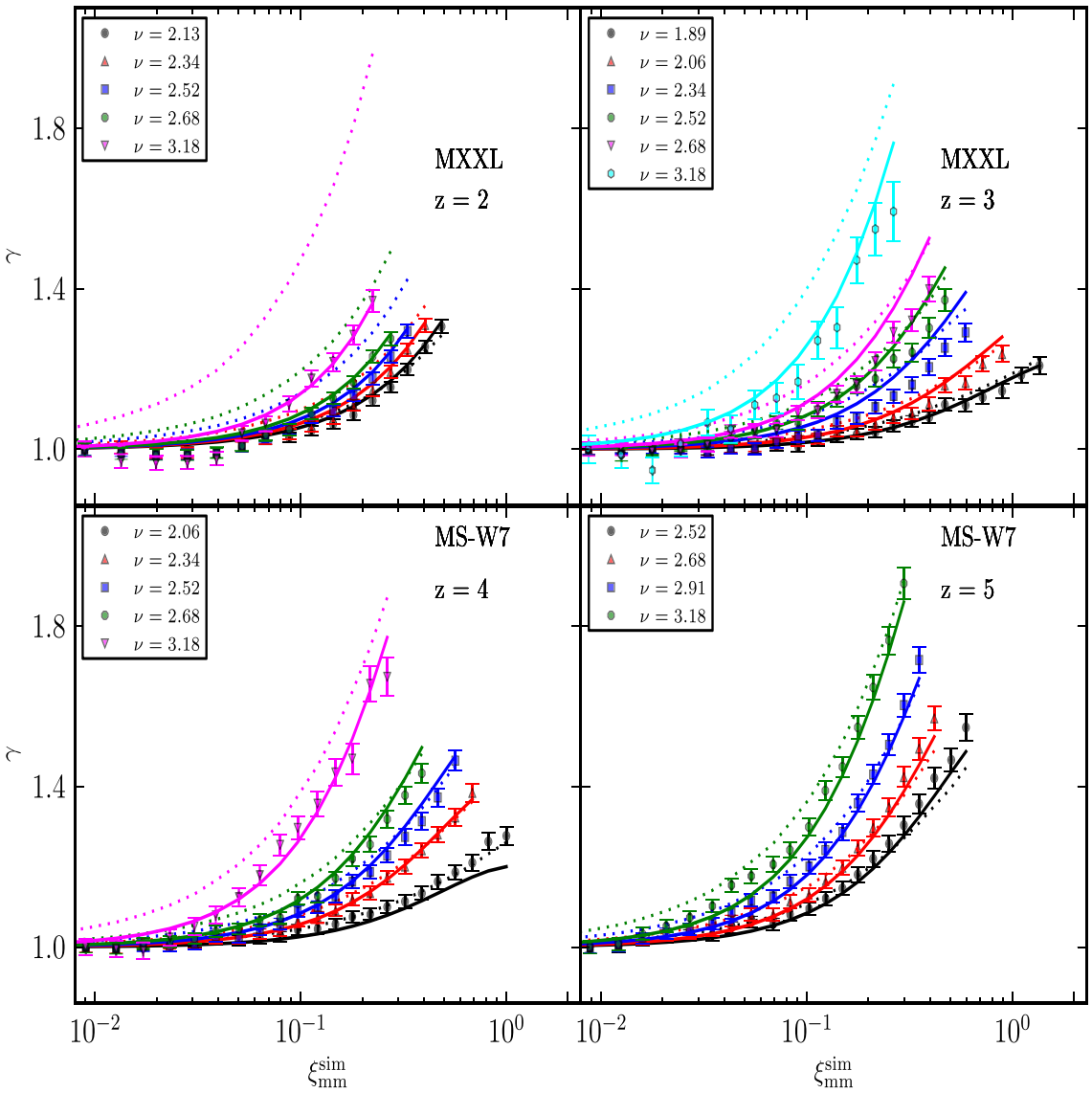

Figure 6. The scale dependence of nonlinear bias, $\gamma(\xi_{\rm mm}^{\rm sim}, \nu, \alpha_{\rm m})$, measured from N-body simulations, in the redshift range $z = 2$–5 as a function of $\xi_{\rm mm}^{\rm sim}(r)$ for haloes in the ν-bins listed in the legend. Solid lines: the fit for $\gamma(\xi_{\rm mm}^{\rm sim}, \nu, \alpha_{\rm m})$ presented in this work. Dotted lines: the fitting function for γ given by Reed et al. (2009).

section, we model halo clustering as a function of the linear matter correlation function, $\xi_{\rm mm}^{\rm lin}(r, z)$. This is well motivated because $\xi_{\rm mm}^{\rm lin}(r, z)$ is easier to compute without uncertainties, compared to the nonlinear matter correlation function. Thus, for all practical purposes, it will be convenient to express the nonlinear bias as a function of $\xi_{\rm mm}^{\rm lin}(r, z)$. The linear matter correlation function is computed from the linear matter power spectrum $P^{\rm lin}(k, z)$ as

$$\xi_{\rm mm}^{\rm lin}(r, z) = \int_0^\infty \frac{{\rm d}k}{2\pi^2} k^2 P^{\rm lin}(k, z) \frac{\sin(kr)}{kr}. \quad (19)$$

In order to model the nonlinear halo bias as a function of $\xi_{\rm mm}^{\rm lin}(r, z)$, we first define $b_{\rm nl}(r, M, z)$ at any given scale as

$$b_{\rm nl}(r, M, z) = \sqrt{\frac{\xi_{\rm hh}^{\rm sim}(r, z)}{\xi_{\rm mm}^{\rm lin}(r, z)}}. \quad (20)$$

The new definition of $b_{\rm nl}(r, M, z)$ is similar to that given by equation (10), but uses $\xi_{\rm mm}^{\rm lin}(r, z)$ instead of $\xi_{\rm mm}^{\rm sim}(r, z)$. Following Section 3.2, we then express the nonlinear bias as the product of the scale-independent large scale bias $b(\nu)$ and the scale-dependent function $\gamma(r, M, z)$ (see equation 11). A new fitting function is obtained for the large scale bias by refitting the free parameters of equation (4) to the large scale bias measured from the simulations. The new best-fitting parameters are given by $A = 1.0$, $a = 0.223$, $B = 1.156$, $b = 2.167$, $C = -0.748$ and $c = 2.167$.

As before, we find that, the scale dependence of halo bias $\gamma(r, M, z)$ can be expressed as a function of ν, $\alpha_{\rm m}$, $\Omega_{\rm m}(z)$ and the linear matter correlation function, $\xi_{\rm mm}^{\rm lin}$. The fitting function for γ is assumed to have the same functional form as in equation (18) with $\xi_{\rm mm}^{\rm sim}$ being replaced by $\xi_{\rm mm}^{\rm lin}$. The free parameters of equation (18) are then determined by fitting this equation to the data measured from all the simulations in the redshift range 0–5. The new best-fitting parameters of equation (18) are given by $K_0 = 0.000529$, $k_1 = 1.0686$, $k_2 = 3.4158$, $k_3 = -204.1715$, $k_4 = 26.9453$, $L_0 = 0.448$, $l_1 = 2.128$, $l_2 = 3.0222$, $l_3 = 0.226$ and $l_4 = 1.691$. We emphasize that the new fit for γ as function of $\xi_{\rm mm}^{\rm lin}$ agrees very well

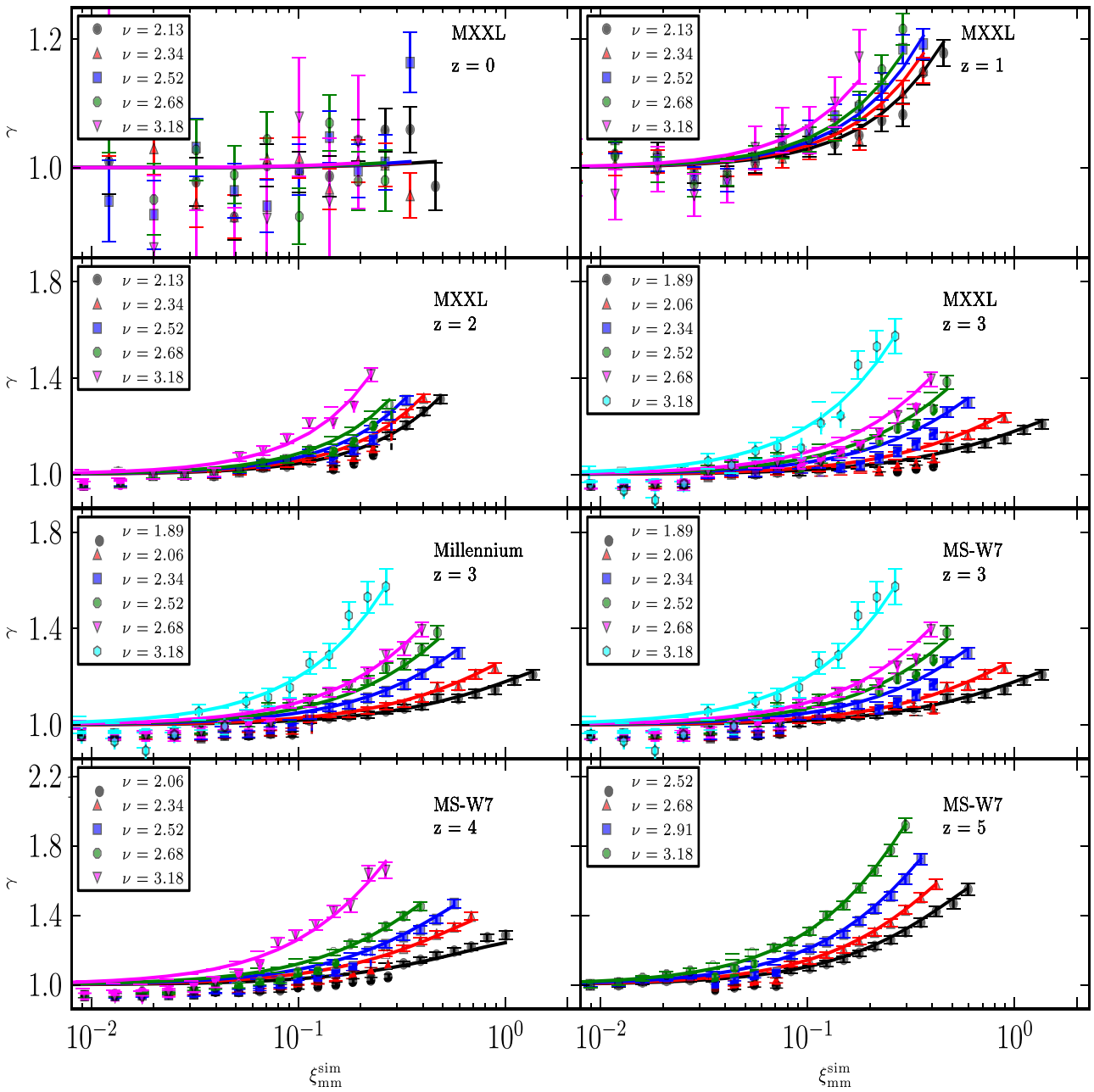

Figure 7. Our fitting function for the scale dependence of the nonlinear bias, $\gamma(\xi_{\rm mm}^{\rm sim}, \nu, \alpha_{\rm m}, \Omega_{\rm m}^{z})$, in the redshift range 0–5 as a function of $\xi_{\rm mm}^{\rm sim}(r)$ for various choices of ν (see legend) is shown using solid lines. The *N*-body simulation from which results were measured along with the redshift is labelled on each panel.

with the simulation data. The overall agreement of this fit with the data from all the simulations given in Table 1 is found to be better than 5 per cent.

4 DISCUSSION AND CONCLUSIONS

We have revisited the problem of modelling the nonlinear clustering of rare dark matter haloes, that collapse from $1\sigma - 3\sigma$ fluctuations, on quasi-linear scales. In particular, we found using high-resolution *N*-body simulations that the nonlinear bias of high redshift galactic dark matter haloes is strongly scale dependent on scales ∼0.5–10 h^{-1} Mpc. These scales, commonly referred to as quasi-linear scales, correspond to scales larger than the typical virial radii of dark matter haloes. Even though we primarily focused on the clustering of dark matter haloes in the redshift range 0–5, our results are applicable to higher redshifts, including the cosmic dark ages before the epoch of reionization.

First, we estimated the correlation functions of dark matter haloes at z =2–5 from the *N*-body simulations, in mass bins in the mass range $10^{11} - 4 \times 10^{12}\,{\rm M}_{\odot}$. These are the typical masses of dark matter haloes that host LBGs and LAEs in the same redshift range and correspond to rarer objects collapsing from high σ fluctuations (Jose et al. 2013b). We then showed that, on quasi-linear scales, there is a strong discrepancy between the halo correlation functions computed using the scale-independent, linear halo bias and those measured directly from simulations. This suggests that the linear bias approximation is not sufficient to explain the clustering of high-z, rarer dark matter haloes on quasi-linear scales.

To quantify the nonlinear bias of dark matter haloes in this redshift range, we measured the correlation functions of haloes, from simulations, in bins of halo peak height, $\nu(M, z)$. The nonlinear bias is defined as the square root of the ratio of halo and dark matter correlation functions (see equation 10). We found that the nonlinear bias of a halo can be expressed as the product of the usual scale-independent large scale bias $b(M, z)$ and a scale-dependent function $\gamma(r, M, z)$ (equation (11)). We also obtained a fitting function for $b(M, z)$ which depends only on the peak height, $\nu(M, z)$, of dark matter haloes. This fit compares very well with other formulae for large scale bias in the literature (Sheth & Tormen 1999; Tinker et al. 2010), especially for haloes with $\nu \lesssim 2$, collapsing from low σ fluctuations. For rarer haloes with larger values of ν, we obtained a slightly lower value for the large scale bias compared to the formula given by Tinker et al. (2010). However, as noted before, this could be due to the difference between the SO and FOF(0.2) halo finder algorithms respectively used by Tinker et al. (2010) and in our work. Further, both studies use distinct simulations with different cosmological parameters for calibrating the bias.

We find that, for $z = 2$–5, the scale dependence of the nonlinear bias, $\gamma(r, M, z)$, for haloes of mass M at any length-scale r depends on three parameters, the peak height, $\nu(M, z)$, of haloes at mass M, the dark matter correlation function ($\xi^{\rm sim}_{\rm mm}(r, z)$) at that length-scale and α_m, an effective power-law index of $\sigma(M)$ at that redshift. We obtained a fitting function that describes the scale dependence of $\gamma(r, M, z)$ as a function of these parameters in the same redshift range. Our fit agrees with the simulation results within an accuracy of 4 per cent.

The scale dependence of nonlinear bias at a scale r is usually parametrized in real space using $\xi^{\rm sim}_{\rm mm}(r, z)$ (Tinker et al. 2005) or the *rms* linear overdensity in uniformly overdense spheres of radius r, $\sigma(r, z)$ (Hamana et al. 2001; Diaferio et al. 2003; Reed et al. 2009). Both $\sigma(r, z)$ and $\xi^{\rm sim}_{\rm mm}(r, z)$ can be expressed as functions of the dark matter power spectrum. However, we find that the scale dependence of the bias, as quantified in terms of $\gamma(r, M, z)$, is not described by such parametrizations, but rather depends on the quantity $\alpha_{\rm m}(z)$. But, to compute $\alpha_{\rm m}(z)$, one requires only the linear dark matter power spectrum. Therefore, it can be argued that at high redshifts ($z \geq 2$) the nonlinear bias is a universal function of the dark matter power spectrum.

We extended our analysis by probing the nonlinear bias of low redshift, rarer dark matter haloes on quasi-linear scales, using MXXL haloes at $z = 0$ and 1. Interestingly at lower redshifts, especially at $z \sim 0$, the scale dependence of nonlinear bias is weaker than at high redshifts and is within 10–20 per cent of the large scale bias measured from simulations at any scale. We propose a fitting function for the nonlinear bias as a function of the matter density of the universe at a given redshift [$\Omega_{\rm m}(z)$] along with $\nu(M, z)$, $\xi^{\rm sim}_{\rm mm}(r, z)$ and $\alpha_{\rm m}(z)$. Remarkably, this fitting function, calibrated using the MS-W7 and MXXL simulations, captures the redshift evolution of nonlinear bias for a wide range of halo masses and length-scales within an overall accuracy of 4 per cent.

The dependence of $\gamma(r, M, z)$ on $\Omega_{\rm m}(z)$ at low redshifts breaks the universality of the nonlinear bias with respect to the linear matter fluctuation field. Thus the observed large scale bias of any galaxy population, which depends only on the dark matter power spectrum through $\nu(M, z)$, will not uniquely determine the scale dependence of the bias. This may provide an opportunity to use the scale dependence of halo bias as a valuable tool to probe cosmology, particularly the matter density of the universe.

We have also extended our analysis by expressing the nonlinear bias as a function of the linear matter correlation function, $\xi^{\rm lin}_{\rm mm}(r, z)$. Here also the nonlinear bias is expressed as the product of the scale-independent large scale bias, $b(M, z)$, and the scale-dependent function, $\gamma(r, M, z)$. We first obtained a fitting function for the large scale bias as a function of $\nu(M, z)$. A fitting function for $\gamma(r, M, z)$ is then obtained as a function of linear matter correlation function, $\xi^{\rm lin}_{\rm mm}(r, z)$, along with $\nu(M, z)$, $\alpha_{\rm m}(z)$ and $\Omega_{\rm m}(z)$. The new fit for γ agrees with the data from the simulations within an accuracy better than 5 per cent. We emphasize that this model parameterizes the clustering of dark matter haloes as a function of $\xi^{\rm lin}_{\rm mm}(r, z)$ instead of the nonlinear matter correlation function. Such a model could be quite useful for practical purposes as it is easier to compute $\xi^{\rm lin}_{\rm mm}(r, z)$ analytically without uncertainties compared to the nonlinear matter correlation function.

In general, the halo bias of high redshift, rare dark matter haloes is significantly nonlinear and scale dependent on quasi-linear scales. On the other hand, at $z = 0$, this scale dependence is quite weak and seems to be dependent on the matter density of the universe. The nonlinear bias is expected to have interesting implications on observations of the high redshift universe. For example, the halo occupation distribution modelling of LBG clustering at high-z ($z \geq 3$) usually assumes a linear halo bias (Hamana et al. 2004, 2006; Hildebrandt et al. 2009; Lee et al. 2009; Jose et al. 2013b). However, at these redshifts, the typical LBGs collapse from 2σ–3σ fluctuations. Hence, one has to incorporate the nonlinear bias to improve the clustering predictions of LBGs on quasi-linear scales. Thus the nonlinear bias could change the predicted shape of the two-point correlations functions of high redshift LBGs and also LAEs, quasars and even the redshifted 21 cm signals from the pre-reionization. It would be interesting to explore the implications of the nonlinear and scale-dependent bias in the high-z universe. To do this, one may need to incorporate the effects of baryons on the clustering of galaxies through the physics of galaxy formation and also of assembly bias. This is left for future work.

ACKNOWLEDGEMENTS

CJ thanks Kandaswamy Subramanian, Raghunathan Srianand and Aseem Paranjpaye for useful discussions. CJ acknowledges partial support from the Institute for Computational Cosmology (ICC), Durham University while visiting the ICC and Carlos Frenk at the ICC for warm hospitality. This work was supported by the Science and Technology Facilities Council [ST/L00075X/1]. This work used the DiRAC Data Centric System at Durham University, operated by the ICC on behalf of the STFC DiRAC HPC Facility (www.dirac.ac.uk). This equipment was funded by BIS National E-infrastructure capital grant ST/K00042X/1, STFC capital grant ST/H008519/1, and STFC DiRAC Operations grant ST/K003267/1 and Durham University. DiRAC is part of the UK's National E-Infrastructure.

REFERENCES

Angulo R. E., Baugh C. M., Frenk C. S., Bower R. G., Jenkins A., Morris S. L., 2005, MNRAS, 362, L25
Angulo R. E., Baugh C. M., Lacey C. G., 2008, MNRAS, 387, 921
Angulo R. E., Springel V., White S. D. M., Jenkins A., Baugh C. M., Frenk C. S., 2012, MNRAS, 426, 2046
Bardeen J. M., Bond J. R., Kaiser N., Szalay A. S., 1986, ApJ, 304, 15
Baumann D., Ferraro S., Green D., Smith K. M., 2013, J. Cosmol. Astropart. Phys., 5, 001
Blanton M., Cen R., Ostriker J. P., Strauss M. A., 1999, ApJ, 522, 590
Bond J. R., Cole S., Efstathiou G., Kaiser N., 1991, ApJ, 379, 440

Boylan-Kolchin M., Springel V., White S. D. M., Jenkins A., Lemson G., 2009, MNRAS, 398, 1150
Cen R., Dong F., Bode P., Ostriker J. P., 2004, preprint (arXiv:astro-ph/0403352)
Cole S. et al., 2005, MNRAS, 362, 505
Cooray A., Sheth R., 2002, Phys. Rep., 372, 1
Davis M., Efstathiou G., Frenk C. S., White S. D. M., 1985, ApJ, 292, 371
Desjacques V., Crocce M., Scoccimarro R., Sheth R. K., 2010, Phys. Rev. D, 82, 103529
Diaferio A., Nusser A., Yoshida N., Sunyaev R. A., 2003, MNRAS, 338, 433
Fry J. N., Gaztanaga E., 1993, ApJ, 413, 447
Gao L., Springel V., White S. D. M., 2005a, MNRAS, 363, L66
Gao L., White S. D. M., Jenkins A., Frenk C. S., Springel V., 2005b, MNRAS, 363, 379
Guo Q., White S., Angulo R. E., Henriques B., Lemson G., Boylan-Kolchin M., Thomas P., Short C., 2013, MNRAS, 428, 1351
Hamana T., Yoshida N., Suto Y., Evrard A. E., 2001, ApJ, 561, L143
Hamana T., Ouchi M., Shimasaku K., Kayo I., Suto Y., 2004, MNRAS, 347, 813
Hamana T., Yamada T., Ouchi M., Iwata I., Kodama T., 2006, MNRAS, 369, 1929
Hildebrandt H., Pielorz J., Erben T., van Waerbeke L., Simon P., Capak P., 2009, A&A, 498, 725
Huff E., Schulz A., White M., Schlegel D., Warren M., 2007, Astropart. Phys., 26, 351
Iliev I. T., Scannapieco E., Martel H., Shapiro P. R., 2003, MNRAS, 341, 81
Jenkins A., Frenk C. S., White S. D. M., Colberg J. M., Cole S., Evrard A. E., Couchman H. M. P., Yoshida N., 2001, MNRAS, 321, 372
Jeong D., Komatsu E., 2009, ApJ, 691, 569
Jose C., Srianand R., Subramanian K., 2013a, MNRAS, 435, 368
Jose C., Subramanian K., Srianand R., Samui S., 2013b, MNRAS, 429, 2333
Kaiser N., 1984, ApJ, 284, L9
Larson D. et al., 2011, ApJS, 192, 16
Lazeyras T., Musso M., Desjacques V., 2016, Phys. Rev. D, 93, 063007
Lee K.-S., Giavalisco M., Conroy C., Wechsler R. H., Ferguson H. C., Somerville R. S., Dickinson M. E., Urry C. M., 2009, ApJ, 695, 368
Manera M., Gaztañaga E., 2011, MNRAS, 415, 383
Matsubara T., 1999, ApJ, 525, 543
McDonald P., Roy A., 2009, J. Cosmol. Astropart. Phys., 8, 020
Mo H. J., White S. D. M., 1996, MNRAS, 282, 347
Musso M., Paranjape A., Sheth R. K., 2013, MNRAS, 427, 3145
Paranjape A., Sefusatti E., Chan K. C., Desjacques V., Monaco P., Sheth R. K., 2013, MNRAS, 436, 449
Peebles P. J. E., 1980, The Large-Scale Structure of the Universe, Princeton Univ. Press, Princeton, NJ
Pike S. R., Kay S. T., Newton R. D. A., Thomas P. A., Jenkins A., 2014, MNRAS, 445, 1774
Pollack J. E., Smith R. E., Porciani C., 2012, MNRAS, 420, 3469
Reed D. S., Bower R., Frenk C. S., Jenkins A., Theuns T., 2009, MNRAS, 394, 624
Scannapieco E., Barkana R., 2002, ApJ, 571, 585
Scannapieco E., Thacker R. J., 2005, ApJ, 619, 1
Seo H., Eisenstein D. J., 2005, ApJ, 633, 575
Sheth R. K., Tormen G., 1999, MNRAS, 308, 119
Sheth R. K., Tormen G., 2004, MNRAS, 350, 1385
Sheth R. K., Mo H. J., Tormen G., 2001, MNRAS, 323, 1
Smith R. E., Marian L., 2011, MNRAS, 418, 729
Smith R. E. et al., 2003, MNRAS, 341, 1311
Smith R., Scoccimarro R., Sheth R., 2007, Phys. Rev. D, 75, 063512
Springel V. et al., 2005, Nature, 435, 629
Tinker J. L., Weinberg D. H., Zheng Z., Zehavi I., 2005, ApJ, 631, 41
Tinker J., Kravtsov A. V., Klypin A., Abazajian K., Warren M., Yepes G., Gottlöber S., Holz D. E., 2008, ApJ, 688, 709
Tinker J. L., Robertson B. E., Kravtsov A. V., Klypin A., Warren M. S., Yepes G., Gottlöber S., 2010, ApJ, 724, 878
van den Bosch F. C., More S., Cacciato M., Mo H., Yang X., 2013, MNRAS, 430, 725

APPENDIX A: THE EFFECTIVE POWER-LAW INDEX OF $\sigma(M)$

For any mass scale M, the variance of smoothed density contrast $\sigma^2(M) \propto k_M^3 P(k_M)\sigma_8^2 k_M^{3+n_{\rm eff}}$ (Peebles 1980). Here $n_{\rm eff}$ is the effective spectral index, which is ~ -2 on galactic scales and -1 on cluster scales. We also have $k_M^{-1} \sim M^{1/3}$. Thus we get

$$\sigma(M) \propto M^{\frac{-(3+n_{\rm eff})}{6}} \propto M^{-\alpha}. \tag{A1}$$

Given the nonlinear mass, $M_{\rm nl}$, and collapse mass, $M_{\rm col}$, corresponds to the mass scales where $\sigma(M)$ is respectively 1 and 1.686, it is possible to define an effective power-law index $\alpha_{\rm m}$ as

$$\frac{\sigma(M_{\rm col})}{\sigma(M_{\rm nl})} = 1.686 = \left(\frac{M_{\rm col}}{M_{\rm nl}}\right)^{-\alpha_{\rm m}} \tag{A2}$$

Thus we have

$$\alpha_{\rm m} = \frac{\log(1.686)}{\log(M_{\rm nl}/M_{\rm col})} = 0.2269\left[\log\frac{M_{\rm nl}}{M_{\rm col}}\right]^{-1}. \tag{A3}$$

This paper has been typeset from a TEX/LATEX file prepared by the author.